THE JOURNAL OF PHYSICAL CHEMISTRY Letters

Letter

pubs.acs.org/JPCL

Liquid Cell Electron Microscopy of Nanoparticle Self-Assembly Driven by Solvent Drying

Won Chul Lee,*[,†,‡,#] Byung Hyo Kim,[§,∥] Sun Choi,[⊥] Shoji Takeuchi,[‡,#] and Jungwon Park*[,§,∥]

[†]Department of Mechanical Engineering, Hanyang University, Ansan, Gyeonggi 15588, Republic of Korea

[‡]Institute of Industrial Science, The University of Tokyo, Tokyo 153-8505, Japan

[#]ERATO Takeuchi Biohybrid Innovation Project, Japan Science and Technology Agency, Tokyo 153-8904, Japan

[§]Center for Nanoparticle Research, Institute for Basic Science (IBS), Seoul 08826, Republic of Korea

[∥]School of Chemical and Biological Engineering, Seoul National University, Seoul 08826, Republic of Korea

[⊥]Center for Urban Energy Research, Korea Institutes of Science and Technology, Seoul 02792, Republic of Korea

Supporting Information

ABSTRACT: Drying a colloidal solution of nanoparticles is a versatile method to construct self-assembled structures of nanoparticles. However, mechanistic understanding has mostly relied on empirical knowledge obtained from the final structures of self-assembly as relevant processes during solvent drying are likely kinetic and far from equilibrium. Here, we present in situ TEM studies of nanoparticle self-assembly under various conditions, including the concentrations of the initial solution and the types of nanoparticles and substrates. The capability of tracking trajectories of individual nanoparticles enables us to understand the mechanisms of drying-mediated self-assembly at the single-nanoparticle level. Our results consistently show that a solvent boundary primarily affects nanoparticle motions and the resulting self-assembly processes regardless of different conditions. The solvent boundary drives nanoparticles to form two-dimensional assembly mainly through two pathways, transporting scattered nanoparticles by lateral dragging and flattening aggregated nanoparticles by vertical pressing.

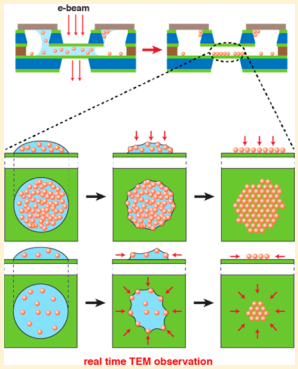

The self-assembly of colloidal nanoparticles provides an opportunity to couple the electronic and physical properties of individual nanocrystals.[1,2] Two- and three-dimensional (2D and 3D) self-assembled structures with a different complexity of their constituent nanocrystals and their arrangements can be constructed in solutions, on substrates, and at interfaces.[1−12] When nanoparticles become equilibrated into self-assembled structures, we can understand and control the processes using particle-to-particle interactions that can be tuned by changing the surface chemistry, sizes, and shapes of nanoparticles in a solution.[3−5] In contrast, nonequilibrium processes become dominant when nanoparticles self-organize onto substrates via the evaporation of a volatile solvent. In this scenario, their motions are strongly affected by kinetic factors such as interactions with a substrate and capillary forces due to solvent evaporation near a substrate; however, these parameters are difficult to estimate and control. Although previous studies[13−23] have successfully demonstrated the formation of ordered 2D superlattices under various conditions, most of these processes were achieved by empirical tuning of kinetic factors[6−12] and are thus difficult to generalize.

Questions are raised in understanding how nonequilibrium drying processes guide individual constituent nanoparticles and produce ordered 2D superlattices under various conditions, including the nanoparticle concentrations and types of nanoparticles, substrates, and solvents. Theoretical approaches have been used to explain how the nucleation and growth of nanoparticle clusters can be affected by the rate of solvent evaporation and resulting motions of nanoparticles near the substrate.[24−28] In experimental approaches, in situ observations have been the leading tools to study nonequilibrium processes of nanoparticle self-assembly at liquid/solid and air/liquid interfaces. In situ optical microscopy[11,22] and X-ray scattering[29−32] provide time-resolved measurements concerning the geometrical distribution of nanoparticle clusters and crystallographic ensemble information about the nanoparticle assembly during solvent evaporation. However, mechanistic studies based on individual nanoparticle trajectories can provide an opportunity to understand the inhomogeneity of nanoparticle motions and their contribution to the overall self-assembly process. Recently, our group demonstrated that liquid cell transmission electron microscopy (TEM)[33−42] can be used to monitor the trajectories of individual nanoparticles during solvent evaporation and improve the mechanistic understanding of the nanoparticle self-assembly.[36] We have shown that solvent evaporation provides major driving forces that lead Pt nanoparticles in a particular concentration to form an assembled domain on a substrate.[36]

Received: December 6, 2016
Accepted: January 17, 2017
Published: January 17, 2017

DOI: 10.1021/acs.jpclett.6b02859
J. Phys. Chem. Lett. 2017, 8, 647−654

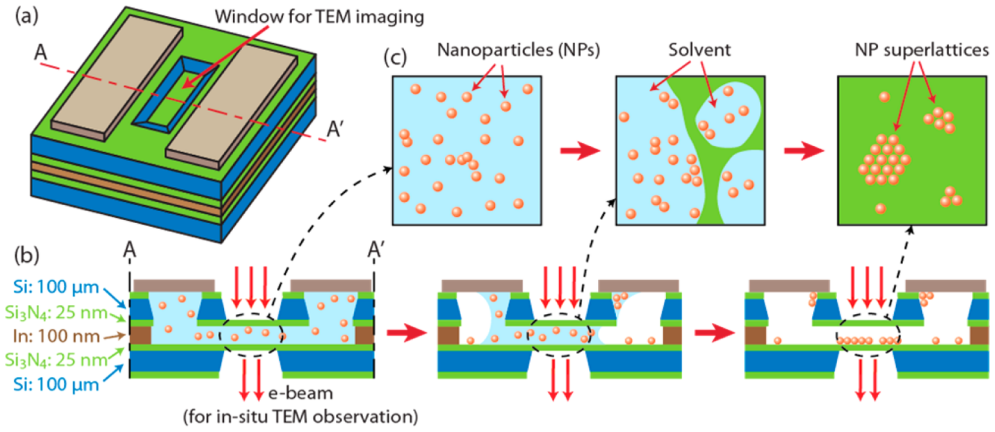

Figure 1. Conceptual illustrations of the liquid cell and in situ TEM imaging. (a) Schematic view of the liquid cell. (b,c) Cross-sectional view of the liquid cell (b) and conceptual illustration of the in situ TEM movie (c) showing 2D self-assembly of nanoparticles under solvent drying.

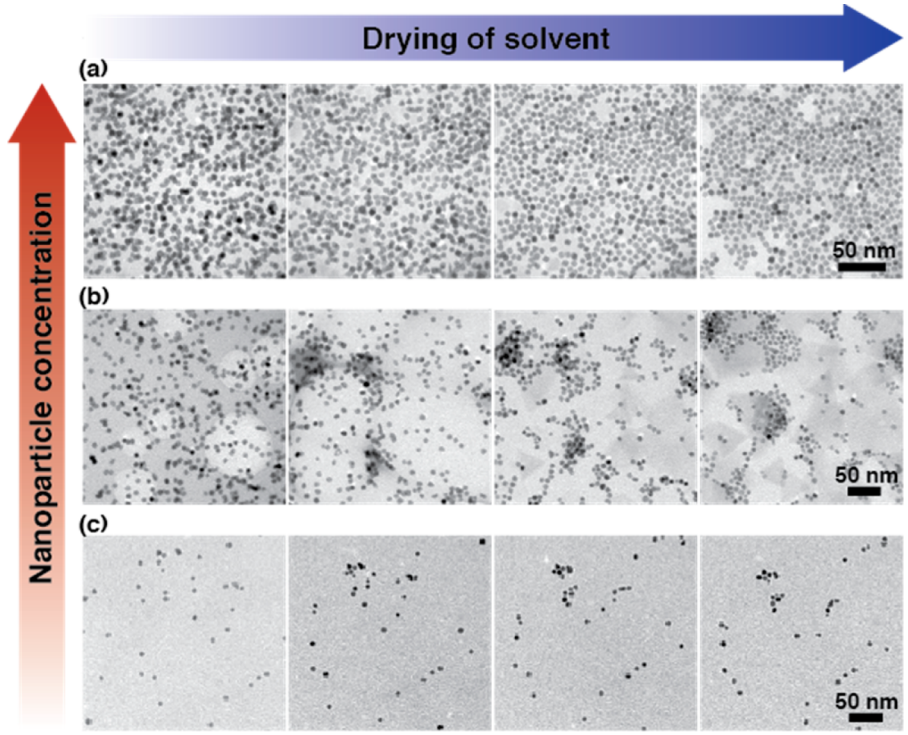

Figure 2. Still snapshots of in situ TEM movies of the solvent-drying-mediated 2D self-assembly in different concentrations of Pt nanoparticles: (a) high concentration, (b) medium concentration, and (c) low concentration. Concentrations between nanoparticle solutions for (a–c) are about 2.5-fold different, consecutively.

Here, we experimentally investigate the mechanisms of 2D nanoparticle self-assembly under various conditions using liquid cell TEM that can resolve single-nanoparticle dynamics. We introduce in situ TEM movies of 2D self-assembly of nanoparticles driven by solvent drying in different particle concentrations, from different types of nanoparticles, and onto different substrates. The liquid-phase TEM in this study (Figure 1) achieves a high level of both spatial and temporal resolution, which is required to directly examine individual nanoparticle trajectories. Tracking individual particles in the movies enables us to understand the crystallization mechanisms at the single-nanoparticle level, which can be easily lost or hidden in ensemble measurements, and to uncover the different roles of solvent evaporation under given conditions. We show that boundaries of drying solvent perform important roles universally, as we reported previously,[36] but they control motions of nanoparticles differently in different assembly conditions.

We captured real-time TEM movies of the 2D self-assembly of inorganic nanoparticles using the liquid cell described in Figure 1 (see the methods in the Supporting Information for detailed preparation steps). Liquid cells were equipped with silicon nitride (SiN_x) windows, which were transparent to the electron beam, and a spacer that limited the maximum thickness of the liquid layer to below 100 nm. We observed the self-assembly of 7.3 nm Pt and 14 nm PbSe nanoparticles while the solvent dried under electron beam irradiation. In addition to using the SiN_x window, which serves as a substrate for superlattice formation, we also varied the substrate by replacing the SiN_x windows with Si windows. Under the given

DOI: 10.1021/acs.jpclett.6b02859
J. Phys. Chem. Lett. 2017, 8, 647–654

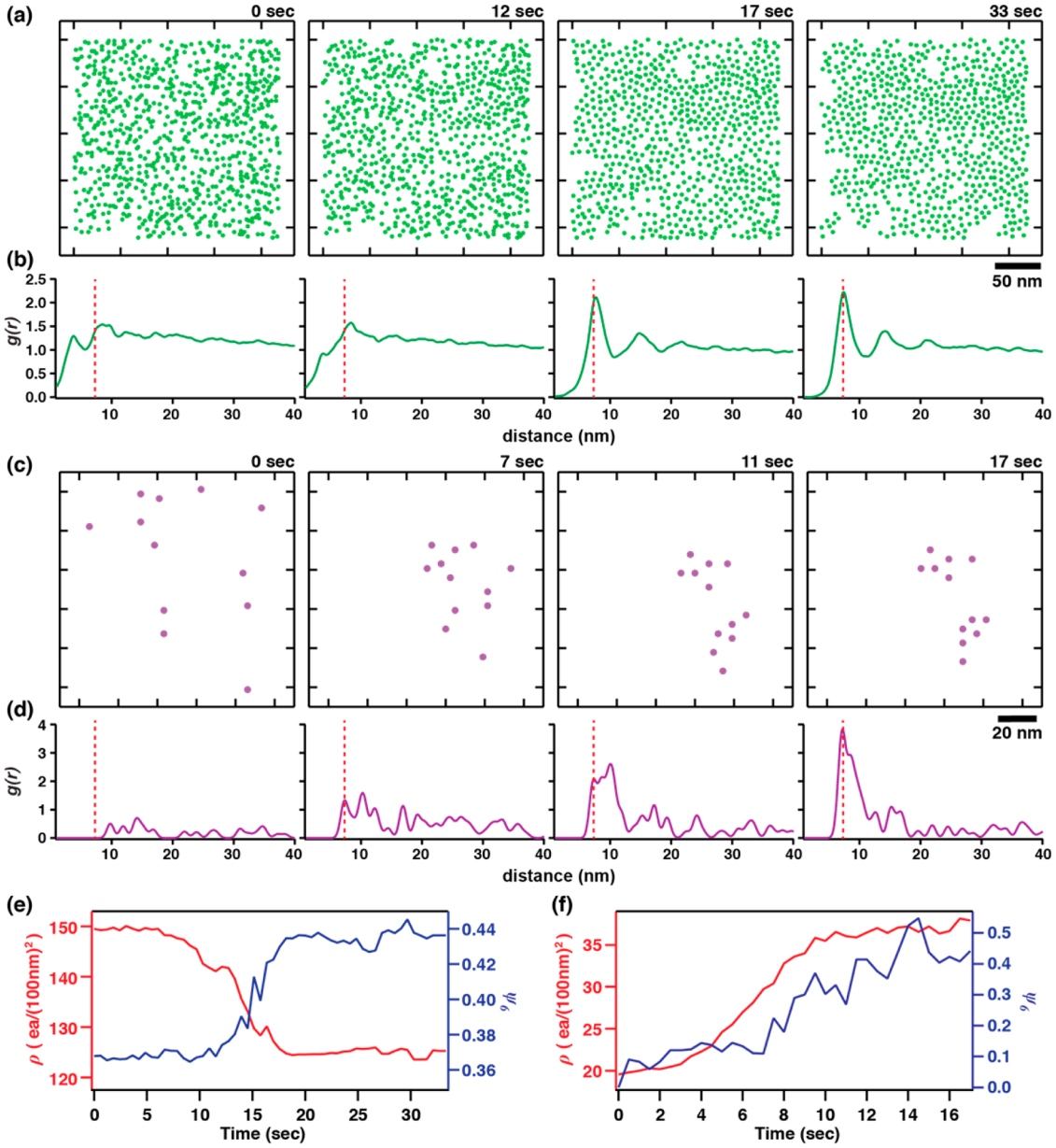

Figure 3. Self-assembly of Pt nanoparticles in high (a,b,e) and low (c,d,f) concentrations. (a,c) Position tracking of individual particles at different times. (b,d) RDFs at different times. The red dashed lines indicate an interparticle distance of 7.3 nm, which represents the average nanoparticle diameter. (e,f) 2D areal density of particles (red) and bond orientational order parameter (blue) plots as a function of time.

experimental conditions, where the thickness of the solvent layer is finite and comparable to the nanoparticle size, solvent dewetting provides a major driving force for nanoparticles to move, and the Brownian-like motions were significantly suppressed.[36] This environment represents the final stage of solvent-drying-mediated self-assembly when nanoparticles are near the substrate.

We first studied how nanoparticles behave differently in solutions with different initial particle concentrations during drying-mediated 2D self-assembly. Figure 2 presents still snapshots from TEM movies of superlattice formation from three nanoparticle solutions with different concentrations. Because of the continuous drying of the solvent from the nanoparticle solutions during the preparation and loading into a liquid cell, loss of a small amount of solvent before imaging is unavoidable. However, as observed in the first images in Figure 2, each nanoparticle solution sample still exhibited an obvious difference in the initial particle density. As the solvent continuously evaporated, the Pt particles within a field of view gradually changed their positions and formed ordered 2D superlattices. The final images for each experiment represent the final 2D superlattices. Because of the different number of particles for each experiment, the coverages of the superlattices were distinct. In the high-concentration experiment, Pt particles covered almost the entire surface, whereas local domains of assembled particles were formed in several spots on the substrate from medium and low concentrations. The particles also followed different types of trajectories and dynamics while the solvent drying mediated the self-assembly.

We analyzed the detailed mechanisms of nanoparticle self-assembly in each concentration control. To follow the trajectories of individual particles, we tracked the 2D projected positions of whole particles within a field of view from the high- and low-concentration experiments (Figure 2a,c and Movies S1

DOI: 10.1021/acs.jpclett.6b02859
J. Phys. Chem. Lett. 2017, 8, 647−654

and S2) as a function of time. Figure 3a,c displays the tracked positions from the two experiments at four different times, with the last time frame for the final superlattice structures. We calculated the radial distribution function (RDF) in Figure 3b,d at different times of the corresponding position diagram to show the distribution of interparticle distances at different stages of nanoparticle self-assembly. Then, we analyzed the temporal change of the 2D areal density, ρ, and 2D bond orientational order parameter,[36] ψ_6, in Figure 3e,f, respectively. ψ_6 represents the degree of crystalline ordering; ψ_6 approaches 1 as a perfectly ordered 2D lattice is evolved and is 0 for a disordered lattice.

At both high and low particle concentrations, nanoparticles were randomly distributed in the earlier states (0 s) and eventually formed ordered superlattices in the final states. This result is directly observed in the position diagrams (Figure 3a,c) and is also supported by the RDFs and 2D bond orientational order parameters. The RDFs exhibit strong peaks near 7.7 nm in the final stages (Figure 3b at 33 s and Figure 3d at 17 s), which indicates that particles are distributed with a regular interparticle distance. The bond orientational order parameters (indices of crystallinity) increase in both cases (the blue lines in Figure 3e,f), which indicates that the particle positions became ordered over time.

Although the two cases are similar in terms of both the positional randomness in the initial stage and the ordered structures in the final stage, their trajectories are distinct, as clearly observed in the changes of the bond orientational order parameters and 2D areal densities. For the high initial concentration, ψ_6 exhibits a steady state over the first 10 s with a low value. Then, the value abruptly increases to a higher value from 12 to 17 s followed by the second steady state. More notably, the 2D areal density exhibits precisely the opposite pattern of the bond orientational order parameter as 2D superlattice formation proceeds. This observation indicates that nanoparticles in a concentrated solution form randomly distributed aggregates in the earlier stage and are rapidly transformed into ordered 2D superlattices at a certain period (12−17 s). However, the low initial concentration experiment revealed gradual increases of both ψ_6 and the areal density over the entire period. The areal density first started to increase, and then, ψ_6 followed with a time lapse of ∼2 s. These results indicate that ordered 2D superlattices are gradually formed by the continuous lateral collection of individual nanoparticles from a diluted solution.

We analyzed nanoparticle motions during the self-assembly process to study how solvent drying generates the two different pathways depending on the nanoparticle concentrations. In the in situ TEM movie under the concentrated solution, the particles formed multiple local clusters in the initial period (0−10 s). This period is also associated with nonzero RDF values at the interparticle distance below the particle diameter (left parts of red dashed lines at 0 and 12 s in Figure 3b), which indicates that particles overlie along the vertical direction. In this initial stage of drying, the areal density and bond orientational order parameter steadily fluctuate, and the particles exhibit local fluctuations until the solvent thickness becomes comparable to the thickness of the particle aggregates. Once the solvent boundary (solvent/vacuum interface) contacts the particle aggregates, the particle/solvent/vacuum contact provides a capillary force that pushes the aggregates downward to the substrate (Figure S4). Particles close to the substrate reorganize their original positions to accommodate particles pushed by the interface from upper positions and to pack particle aggregates into one monolayer. The abrupt changes of the areal density and bond orientational order parameter directly confirm that particles find ordered positions during this step. The small mean-square displacement (MSD) in Figure S2 is also consistent with this observation because such vertical motions of nanoparticles are excluded and only weak lateral motions are included in the 2D projected position tracking. During the last stage of solvent drying, the solvent level becomes less than one particle thickness; thus, solvent dragging by the substrate/solvent/vacuum interface causes fluctuation of the particles within one monolayer and refines the individual particle positions in the final superlattice. This stage, where the areal density and bond orientational order parameter only undergo minor fluctuations, can be seen from the contrast fluctuation of particles in static positions in Movie S1.

During the initial stage from the diluted solution, the position diagram and RDF show that nanoparticles scatter at random positions with large interparticle distances as opposed to the formation of local aggregates in the concentrated solution. As the solvent dries, the solvent boundary drags particles laterally over a long distance from their original positions, and particles gradually form ordered clusters within 17 s. The MSDs and trajectories in Figure S3 confirm these long lateral motions of nanoparticles, which are different from the concentrated case. The lateral motions of particles are slow during the initial stage and then become rapid from 4 to 10 s. The areal density plot also exhibits similar behavior. During the early stage of solvent drying, the particles are immersed in the solvent; thus, the solvent front drags particles less effectively. As the solvent boundary contacts particles, forming the particle/solvent/vacuum interface, the solvent boundary actively brings particles close to each other and forms small ordered domains. The gradual evolution of order causes the increase in the bond orientational order parameter (Figure 3f).

Comparing the two different pathways of superlattice formation from solutions with high and low particle concentrations, the solvent boundary acts as the major driving factor for both cases; however, its effects are clearly different. When particles are in concentrated solution, the solvent boundary flattens aggregated particles downward to form the wide 2D ordered assembly on the substrate. However, the solvent boundary in a dilute solution mostly drags particles laterally, forming local domains of ordered particle islands.

In the previous paragraphs, we discussed the two different pathways of self-assembly from solutions with high and low concentrations. These two distinct mechanisms are nested sequentially in multiple steps of the solvent-drying-mediated 2D self-assembly that we discussed in our previous report,[36] whose particle concentration is likely between the two cases that we discussed in the previous paragraphs. Briefly, the drying solvent first pushes the particle laterally to form amorphous aggregates during the earlier stage and pushes down the aggregates to flatten as ordered domains of particles onto the substrate during the later stage. These observations entice us to revisit 2D superlattice formation in a particle concentration between the two opposite cases that we discussed to elucidate how two major effects by the solvent boundary cooperate in the midregime of the particle concentration and to understand the formation mechanism at a single-particle trajectory level. We calculated a local value of the 2D areal density near each particle and divide the particles into two groups that have higher and lower values of the local areal density (see the

DOI: 10.1021/acs.jpclett.6b02859
J. Phys. Chem. Lett. 2017, 8, 647−654

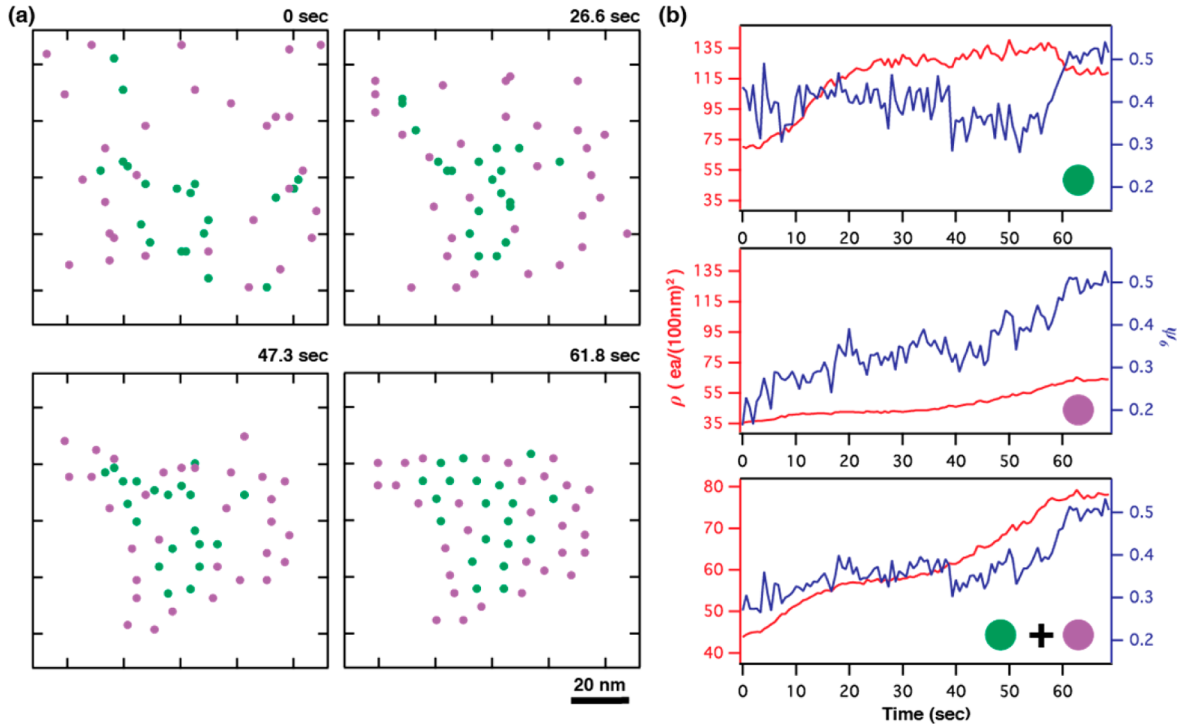

Figure 4. Self-assembly of Pt nanoparticles in a medium concentration. (a) Position tracking of individual particles at different times of solvent drying. The particles are identified in two different groups that have higher (green) and lower (purple) values of the local areal density near each particle. (b) 2D areal density of particles (red) and a bond orientational order parameter (blue) plotted as a function of time. Separate plots for the two different groups are shown (top: green; middle: purple) along with a plot for all of the particles (bottom).

methods in the Supporting Information for details). The two different groups of particles are tracked with respect to the 2D projected positions, and Figure 4a shows them with green (higher density) and purple (lower density) dots. Regardless of the green and purple groups, all of the particles are located at randomly distributed positions at the beginning of the solvent drying and eventually form one large ordered domain. However, tracking the trajectories of individual constituent particles uncovers differences. Figure 4b presents the areal density and bond orientational order plots for these two groups of particles. The green and purple particles exhibit distinct behaviors. First, the green particles experience an increase of the areal density during the early stage and maintain the high density for a prolonged period, followed by a sudden drop after 55 s. More notably, this sudden drop coincides with the jump of the bond orientational order parameter. This crossover during the final stage is consistent with our observation from the experiment with the concentrated solution (Figures 2a and 3a,b,e). Green particles are likely to form densely packed agglomerates in the early stage, which continue dynamic motions without developing order. Eventually, when the solvent drying pushes agglomerated particles onto the substrate, particles rapidly settle down in ordered positions with a regular interparticle distance, which turns out to be the crossover of the areal density and bond orientational order parameter at the final stage. In contrast, the purple particles exhibit gradual growth of these two plots throughout the self-assembly process. This behavior indicates that the particles approach each other and evolve their order as the particles are gradually dragged by the solvent boundary. The trajectories from the diluted particle concentration (Figures 2c and 3c,d,f) actually reflect a similar pattern during superlattice formation. Thus, our observations confirm that the drying solvent boundary either flattens densely packed particles onto the substrate or laterally assembles distributed particles in a single drying process, and the degree of these two major roles differs depending on how the particles are crowded.

We further expect that solvent dragging can provide a general driving force for the motions of different types of nanoparticles with a similar size range near the substrate. We observed the drying-mediated motions of 14 nm PbSe nanoparticles using the same SiN_x liquid cell using TEM. We synthesized PbSe nanoparticles (see the Supporting Information) and redispersed them in the identical solvent as that for the Pt particle solution. We prepared a TEM movie (Movie S3) of PbSe nanoparticles moving in the vicinity of where the solvent drying boundary proceeds. In TEM still snapshots (Figure 5a) of the in situ movie, five PbSe particles that experience effective lateral transport by the solvent boundary are marked with colored circles as a visible aid. Five PbSe particles are strongly pushed to the direction in which the solvent boundary continuously proceeds during drying (Figure 5b). Eventually, four particles form a linear alignment, whereas the other particle is left in a separate location. The contribution of solvent dragging for the lateral movements of PbSe particles is consistent with our previous observation in the 2D self-assembly of Pt particles from a low-concentration solution. We also observed that particles within the large domain, the upper right side of the TEM images in Figure 5a, are loosely packed at the beginning of the solvent drying. As the solvent drying boundary passes over the boundary of the particle domain, it pushes and rotates individual particles such that they are tightly packed and locked in the domain. Thus, the nanoparticles form a tightly packed ordered domain when the solvent drying is completed. In the previous study of Pt superlattice formation,[36] we observed similar translational and rotational motions of single particles

DOI: 10.1021/acs.jpclett.6b02859
J. Phys. Chem. Lett. 2017, 8, 647−654

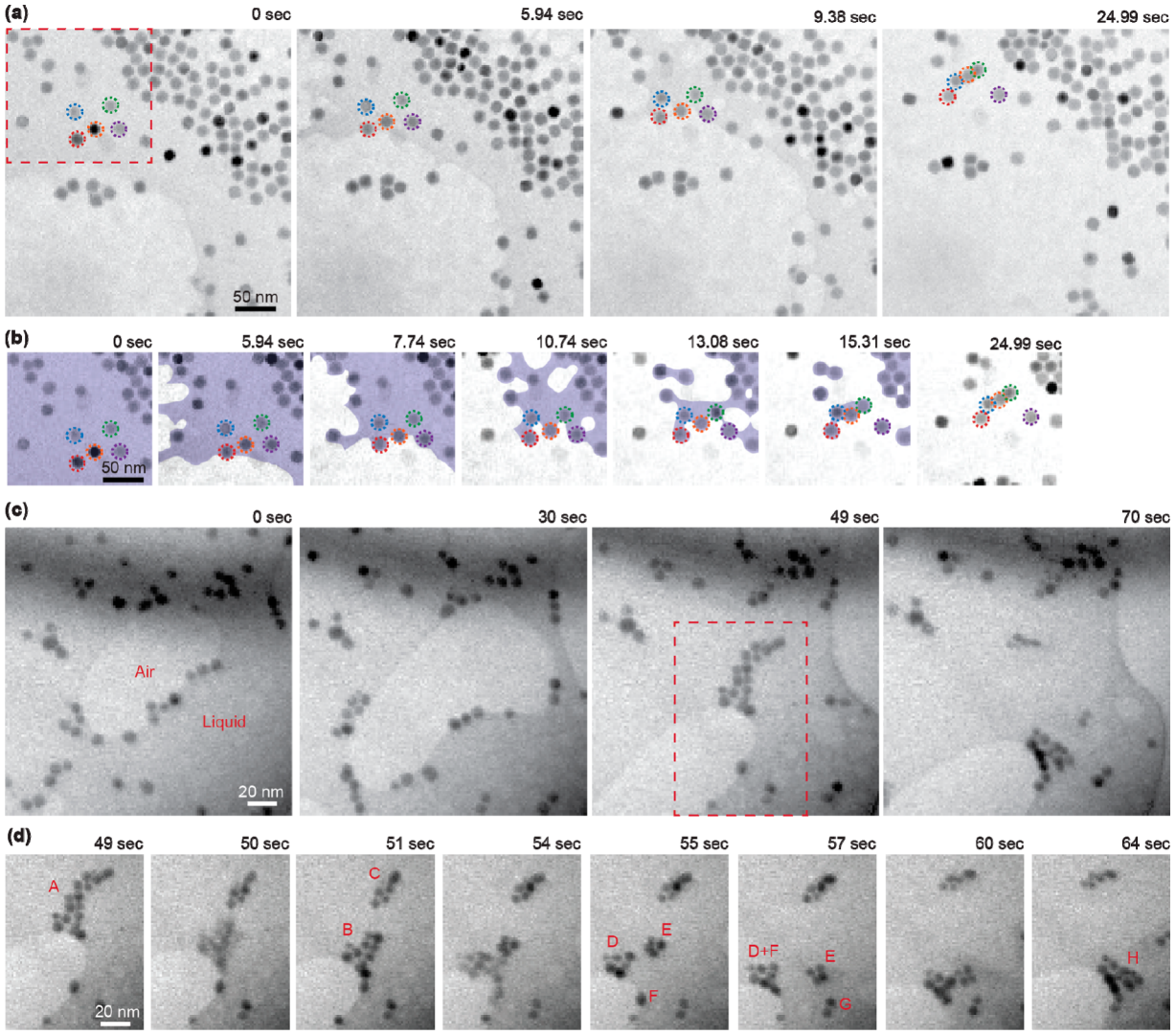

Figure 5. Still snapshots of in situ TEM observation of drying-mediated motions of nanoparticles. (a) PbSe nanoparticle motion on a SiN_x substrate. Five PbSe particles that experience distinct dragging by the solvent boundary are marked with colored circles. (b) TEM images that show the five nearby PbSe particles. Regions that are wet by the solvent are shown with the purple color overlay. (c) Pt nanoparticle motion on a Si substrate. (d) Enlarged still snapshots of the square part outlined by the dashed line in (c). The nanoparticle domain A divides into domains B and C; then, domain B divides into domains D−F, and finally, domains D−G merge into domain H.

induced by the solvent boundary to fill in the space near preordered domains. It is interesting to note that oleic acid capped PbSe nanoparticles show similar behavior with oleylamine capped Pt nanoparticles. It is presumably because floppy long alkyl chains of both oleic acid and oleylamine protrude out of nanoparticles and have dominant interactions with the solvent boundary that determine overall nanoparticle motions. This observation further suggests that nanoparticles with different extending functional groups on surfaces may have different types of interactions and show different motions during solvent evaporation.

To investigate the effect of substrate types on particle behaviors, we prepared a different type of liquid cell with imaging windows made of silicon (see the methods in the Supporting Information and Figure S5 for details) and performed in situ TEM examination of Pt nanoparticles in the same solvent system and imaging environment. TEM still snapshots of the in situ movie (Movie S4) are presented in Figure 5c, and the TEM image of assembled Pt nanoparticles after solvent evaporation in the liquid cell is shown in Figure S6. The wetted and dried areas are distinguished by the dark and bright background contrasts, respectively. During observation under electron beam irradiation, fluctuation of the solvent boundary was clearly visible. The solvent boundary, as we consistently observed in many different cases throughout this work, dragged particles to the area still wetted by the solvent as well as moving particles in the direction in which the solvent boundary progressed. However, we note a few distinct behaviors of particles on the silicon substrate, which are different from those of the SiN_x window liquid cell experiment. First, the particles exhibit continuous local fluctuation. On the SiN_x substrate, nanoparticles are strongly perturbed by the substrate interaction and frequently exhibit step jump motion.[38,39] Pt nanoparticles on the Si window, however, exhibit continuous fluctuation within the solvent between the moments where they are moved over a long distance by the solvent dragging force. In addition, preformed groups of several particles (small 2D domains) are frequently observed within the wet area that is not yet swept by the solvent boundary. The small domains indeed merge and divide continuously by

DOI: 10.1021/acs.jpclett.6b02859
J. Phys. Chem. Lett. 2017, 8, 647−654

following fluctuations of the solvent boundary (Figure 5d). Such events that represent the high mobility of nanoparticles are frequently observed near the solvent drying boundary, which implies that the solvent boundary still provides a major driving force for particle motions and their assembly even if the particles have weak interactions with the substrate.

It is also worth noting that the faster and more continuous motion of nanoparticles on Si substrates is most likely due to the lower surface roughness and reduced charging effect of the Si substrate compared with those of SiN_x. First, Si substrates have a smoother surface than SiN_x, which presumably promotes less perturbed particle dynamics (see more description in the Supporting Information and Figure S7). Second, the continuous motion of nanoparticles in a Si liquid cell can also be affected by the different charge statuses of Si and SiN_x liquid cells under electron beam irradiation. In the case of dielectric SiN_x, local charges generated by the electron beam are accumulated, inducing additional particle−substrate interaction.[39−41] The localized interaction can cause a step jump motion with slow movement.[38,39] On the other hand, the induced charges of Si liquid cells may easily dissipate due to the high electron mobility of Si. Therefore, the translational motion of nanoparticles in Si liquid cells is faster and more continuous than that in SiN_x liquid cells. Our observation using Si liquid cells opens up the possibility of tracking the intact motions of nanoparticles in liquid by reducing particle−substrate interaction.

The drying condition in liquid cell TEM is undoubtedly not identical to the experimental condition of nanoparticle self-assembly in an ambient environment. In addition, it is apparent that an electron beam would perturb the chemical properties of the solvent in the high-dose condition the we used in this experiment. Likewise, thermodynamic factors, including the interface free energy and particle-to-particle interaction, would also contribute mechanisms to the resulting nanoparticle assembly. However, in situ TEM observations of nanoparticle self-assembly in this study confirm that the boundary of the drying solvent generally plays an important role for nanoparticle self-assembly under many different conditions. Because the formation and movement of the solvent boundary indicate solvent fluctuations previously defined as changes of the local density of the solvent on the length scale of the nanoparticles during solvent evaporation, the observations in this study are consistent with the previous theoretical expectations that solvent fluctuations strongly affect nanoparticle motion and determine the final self-assembly structure.[24−28] The situation that we observe in this experiment most likely corresponds to the final stage of particle self-assembly on the substrate that we perform under ambient solvent drying conditions. Indeed, we observe the similarity of the final assembled structures from in situ TEM experiments and drying methods under ambient conditions. In addition to the Pt particle superlattices that we compared in the previous study,[36] 2D superlattices of Au and PbSe nanoparticles are formed on the same Si_3N_4 substrate under natural drying at ambient pressure. TEM images of such structures are presented in Figure S8. Superlattices formed from drying of particle solutions with low and high concentrations contain local domains composed of a few particles and an ordered monolayer over a long range, respectively. Similar structural details are also observed when 2D superlattices of particles are formed on a carbon film. 2D superlattices of different types of particles (Au, PbS, and PbSe) from different concentrations can be observed in the TEM images in Figure S9.

We report direct observations of nanoparticle self-assembly on solid substrates using in situ liquid-phase TEM. The observation with the ability to distinguish the trajectories of individual particles elucidates two major motions provided by solvent drying: dragging laterally scattered particles and flattening locally aggregated particles. In addition, we observed that lateral dragging acts as the major driving force for particles to form a 2D superlattice in a low concentration, whereas flattening particles onto the substrate by solvent boundaries becomes more dominant as the particle concentration increases. We also observed that this solvent boundary mechanism is commonly observed in the 2D self-assembly of different types of nanoparticles and substrates. A fundamental understanding regarding 2D superlattice formation as well as the technical development for in situ TEM imaging that we present here will be utilized in many fundamental studies that require real-time observation with nanoscale resolution.

■ ASSOCIATED CONTENT

Supporting Information

The Supporting Information is available free of charge on the ACS Publications website at DOI: 10.1021/acs.jpclett.6b02859.

Movie of the self-assembly from high-concentration experiments (AVI)

Movie of the self-assembly from low-concentration experiments (AVI)

TEM movie of PbSe nanoparticles (AVI)

TEM movie of Pt nanoparticles on a Si substrate (AVI)

Experimental and analysis methods and supporting figures (PDF)

■ AUTHOR INFORMATION

Corresponding Authors

*E-mail: wonchullee@hanyang.ac.kr (W.C.L.).

*E-mail: jungwonpark@snu.ac.kr (J.P.).

ORCID

Won Chul Lee: 0000-0001-8479-0836

Shoji Takeuchi: 0000-0001-6946-0409

Jungwon Park: 0000-0003-2927-4331

Notes

The authors declare no competing financial interest.

■ ACKNOWLEDGMENTS

We thank Prof. A. Paul Alivisatos at the University of California, Berkeley and Prof. Taeghwan Hyeon at Seoul National University for helpful discussion. This work was supported by IBS-R006-D1. W.C.L. gratefully acknowledges support from the Basic Science Research Program and the Convergence Technology Development Program for Bionic Arm through the National Research Foundation of Korea (NRF) funded by the Ministry of Science, ICT & Future Planning (2016R1C1B1014940 and 2015M3C1B2052811). S.T. and W.C.L. gratefully acknowledge support from the Takeuchi Biohybrid Innovation Project, Exploratory Research for Advanced Technology (ERATO), Japan Science and Technology (JST). S.C. gratefully acknowledges support from the KIST Institutional Program (Project No. 2E27050).

DOI: 10.1021/acs.jpclett.6b02859
J. Phys. Chem. Lett. 2017, 8, 647−654

REFERENCES

(1) Talapin, D. V.; Lee, J.-S.; Kovalenko, M. V.; Shevchenko, E. V. Prospects of Colloidal Nanocrystals for Electronic and Optoelectronic Applications. *Chem. Rev.* **2010**, *110*, 389−458.

(2) Pileni, M. P. Self-Assembly of Inorganic Nanocrystals: Fabrication and Collective Intrinsic Properties. *Acc. Chem. Res.* **2007**, *40*, 685−693.

(3) Shevchenko, E. V.; Talapin, D. V.; Kotov, N. A.; O'Brien, S.; Murray, C. B. Structural Diversity in Binary Nanoparticle Superlattices. *Nature* **2006**, *439*, 55−59.

(4) Talapin, D. V.; Shevchenko, E. V.; Bodnarchuk, M. I.; Ye, X.; Chen, J.; Murray, C. B. Quasicrystalline Order in Self-Assembled Binary Nanoparticle Superlattices. *Nature* **2009**, *461*, 964−967.

(5) Evers, W. H.; Friedrich, H.; Filion, L.; Dijkstra, M.; Vanmaekelbergh, D. Observation of a Ternary Nanocrystal Superlattice and Its Structural Characterization by Electron Tomography. *Angew. Chem., Int. Ed.* **2009**, *48*, 9655−9657.

(6) Han, W.; Lin, Z. Learning From "coffee Rings": Ordered Structures Enabled by Controlled Evaporative Self-Assembly. *Angew. Chem., Int. Ed.* **2012**, *51*, 1534−1546.

(7) van Roekel, H. W. H.; Stals, P. J. M.; Gillissen, M. A. J.; Hilbers, P. A. J.; Markvoort, A. J.; de Greef, T. F. A. Evaporative Self-Assembly of Single-Chain, Polymeric Nanoparticles. *Chem. Commun.* **2013**, *49*, 3122−3124.

(8) Han, W.; Byun, M.; Lin, Z. Assembling and Positioning Latex Nanoparticles via Controlled Evaporative Self-Assembly. *J. Mater. Chem.* **2011**, *21*, 16968−16972.

(9) Stannard, A. Dewetting-Mediated Pattern Formation in Nanoparticle Assemblies. *J. Phys.: Condens. Matter* **2011**, *23*, 083001.

(10) Yang, L.; Gao, K.; Luo, Y.; Luo, J.; Li, D.; Meng, Q. In Situ Observation and Measurement of Evaporation-Induced Self-Assembly under Controlled Pressure and Temperature. *Langmuir* **2011**, *27*, 1700−1706.

(11) Bigioni, T. P.; Lin, X.-M.; Nguyen, T. T.; Corwin, E. I.; Witten, T. A.; Jaeger, H. M. Kinetically Driven Self Assembly of Highly Ordered Nanoparticle Monolayers. *Nat. Mater.* **2006**, *5*, 265−270.

(12) Choi, S.; Jamshidi, A.; Seok, T. J.; Wu, M. C.; Zohdi, T. I.; Pisano, A. P. Fast, High-Throughput Creation of Size-Tunable Micro/nanoparticle Clusters via Evaporative Self-Assembly in Picoliter-Scale Droplets of Particle Suspension. *Langmuir* **2012**, *28*, 3102−3111.

(13) Tang, J.; Ge, G.; Brus, L. E. Gas-Liquid-Solid Phase Transition Model for Two-Dimensional Nanocrystal Self-Assembly on Graphite. *J. Phys. Chem. B* **2002**, *106*, 5653−5658.

(14) Maillard, M.; Motte, L.; Pileni, M. P. Rings and Hexagons Made of Nanocrystals. *Adv. Mater.* **2001**, *13*, 200−204.

(15) Ge, G.; Brus, L. Evidence for Spinodal Phase Separation in Two-Dimensional Nanocrystal Self-Assembly. *J. Phys. Chem. B* **2000**, *104*, 9573−9575.

(16) Stannard, A.; Martin, C. P.; Pauliac-Vaujour, E.; Moriarty, P.; Thiele, U. Dual-Scale Pattern Formation in Nanoparticle Assemblies. *J. Phys. Chem. C* **2008**, *112*, 15195−15203.

(17) Stannard, A.; Alhummiany, H.; Pauliac-Vaujour, E.; Sharp, J. S.; Moriarty, P.; Thiele, U. Directing the Formation of Nanostructured Rings via Local Oxidation. *Langmuir* **2010**, *26*, 13892−13896.

(18) Stowell, C.; Korgel, B. A. Self-Assembled Honeycomb Networks of Gold Nanocrystals. *Nano Lett.* **2001**, *1*, 595−600.

(19) Martin, C. P.; Blunt, M. O.; Moriarty, P. Nanoparticle Networks on Silicon: Self-Organized or Disorganized? *Nano Lett.* **2004**, *4*, 2389−2392.

(20) Blunt, M. O.; Martin, C. P.; Ahola-Tuomi, M.; Pauliac-Vaujour, E.; Sharp, P.; Nativo, P.; Brust, M.; Moriarty, P. J. Coerced Mechanical Coarsening of Nanoparticle Assemblies. *Nat. Nanotechnol.* **2007**, *2*, 167−170.

(21) Govor, L. V.; Reiter, G.; Parisi, J.; Bauer, G. H. Self-Assembled Nanoparticle Deposits Formed at the Contact Line of Evaporating Micrometer-Size Droplets. *Phys. Rev. E* **2004**, *69*, 61609.

(22) Pauliac-Vaujour, E.; Stannard, A.; Martin, C. P.; Blunt, M. O.; Notingher, I.; Moriarty, P. J.; Vancea, I.; Thiele, U. Fingering Instabilities in Dewetting Nanofluids. *Phys. Rev. Lett.* **2008**, *100*, 176102.

(23) Ohara, P. C.; Heath, J. R.; Gelbart, W. M. Self-Assembly of Submicrometer Rings of Particles from Solutions of Nanoparticles. *Angew. Chem., Int. Ed. Engl.* **1997**, *36*, 1078−1080.

(24) Kletenik-Edelman, O.; Ploshnik, E.; Salant, A.; Shenhar, R.; Banin, U.; Rabani, E. Drying-Mediated Hierarchical Self-Assembly of Nanoparticles: A Dynamical Coarse-Grained Approach. *J. Phys. Chem. C* **2008**, *112*, 4498−4506.

(25) Yosef, G.; Rabani, E. Self-Assembly of Nanoparticles into Rings: A Lattice-Gas Model. *J. Phys. Chem. B* **2006**, *110*, 20965−20972.

(26) Kletenik-Edelman, O.; Sztrum-Vartash, C. G.; Rabani, E. Coarse-Grained Lattice Models for Drying-Mediated Self-Assembly of Nanoparticles. *J. Mater. Chem.* **2009**, *19*, 2872−2876.

(27) Sztrum, C. G.; Rabani, E. Out-of-Equilibrium Self-Assembly of Binary Mixtures of Nanoparticles. *Adv. Mater.* **2006**, *18*, 565−571.

(28) Rabani, E.; Reichman, D. R.; Geissler, P. L.; Brus, L. E. Drying-Mediated Self-Assembly of Nanoparticles. *Nature* **2003**, *426*, 271−274.

(29) Loubat, A.; Impéror-Clerc, M.; Pansu, B.; Meneau, F.; Raquet, B.; Viau, G.; Lacroix, L. M. Growth and Self-Assembly of Ultrathin Au Nanowires into Expanded Hexagonal Superlattice Studied by in Situ SAXS. *Langmuir* **2014**, *30*, 4005−4012.

(30) Connolly, S.; Fullam, S.; Korgel, B.; Fitzmaurice, D. Time-Resolved Small-Angle X-Ray Scattering Studies of Nanocrystal Superlattice Self-Assembly. *J. Am. Chem. Soc.* **1998**, *120*, 2969−2970.

(31) Lu, C.; Akey, A. J.; Dahlman, C. J.; Zhang, D.; Herman, I. P. Resolving the Growth of 3D Colloidal Nanoparticle Superlattices by Real-Time Small-Angle X-Ray Scattering. *J. Am. Chem. Soc.* **2012**, *134*, 18732−18738.

(32) Bokhonov, B. B.; Sharafutdinov, M. R.; Whitcomb, D. R.; Burleva, L. P. In Situ Self-Assembly of Silver Nanoparticles. *J. Phys. Chem. C* **2014**, *118*, 11980−11989.

(33) Jungjohann, K. L.; Bliznakov, S.; Sutter, P. W.; Stach, E. A.; Sutter, E. A. In Situ Liquid Cell Electron Microscopy of the Solution Growth of Au-Pd Core-Shell Nanostructures. *Nano Lett.* **2013**, *13*, 2964−2970.

(34) Yu, X. Y.; Liu, B.; Yang, L. Imaging Liquids Using Microfluidic Cells. *Microfluid. Nanofluid.* **2013**, *15*, 725−744.

(35) Yuk, J. M.; Park, J.; Ercius, P.; Kim, K.; Hellebusch, D. J.; Crommie, M. F.; Lee, J. Y.; Zettl, A.; Alivisatos, a P. High-Resolution EM of Colloidal Nanocrystal Growth Using Graphene Liquid Cells. *Science* **2012**, *336*, 61−64.

(36) Park, J.; Zheng, H.; Lee, W. C.; Geissler, P. L.; Rabani, E.; Alivisatos, A. P. Direct Observation of Nanoparticle Superlattice Formation by Using Liquid Cell Transmission Electron Microscopy. *ACS Nano* **2012**, *6*, 2078−2085.

(37) Park, J.; Elmlund, H.; Ercius, P.; Yuk, J. M.; Limmer, D. T.; Chen, Q.; Kim, K.; Han, S. H.; Weitz, D. A.; Zettl, A.; Alivisatos, A. P. 3D Structure of Individual Nanocrystals in Solution by Electron Microscopy. *Science* **2015**, *349*, 290−295.

(38) Zheng, H.; Claridge, S. A.; Minor, A. M.; Alivisatos, A. P.; Dahmen, U. Nanocrystal Diffusion in a Liquid Thin Film Observed by in Situ Transmission Electron Microscopy. *Nano Lett.* **2009**, *9*, 2460−2465.

(39) Chee, S. W.; Baraissov, Z.; Loh, N. D.; Matsudaira, P. T.; Mirsaidov, U. Desorption-Mediated Motion of Nanoparticles at the Liquid-Solid Interface. *J. Phys. Chem. C* **2016**, *120*, 20462−20470.

(40) Liu, Y.; Lin, X.-M.; Sun, Y.; Rajh, T. In Situ Visualization of Self-Assembly of Charged Gold Nanoparticles. *J. Am. Chem. Soc.* **2013**, *135*, 3764−3767.

(41) Verch, A.; Pfaff, M.; de Jonge, N. Exceptionally Slow Movement of Gold Nanoparticles at a Solid/Liquid Interface Investigated by Scanning Transmission Electron Microscopy. *Langmuir* **2015**, *31*, 6956−6964.

(42) Sutter, E.; Sutter, P.; Tkachenko, A. V.; Krahne, R.; de Graaf, J.; Arciniegas, M.; Manna, L. In Situ Microscopy of the Self-Assembly of Branched Nanocrystals in Solution. *Nat. Commun.* **2016**, *7*, 11213.

DOI: 10.1021/acs.jpclett.6b02859
J. Phys. Chem. Lett. 2017, 8, 647−654